IEEE Access
Multidisciplinary | Rapid Review | Open Access Journal

Received June 18, 2021, accepted July 31, 2021, date of publication August 9, 2021, date of current version August 16, 2021.

*Digital Object Identifier 10.1109/ACCESS.2021.3103388*

# Self-Powered Photovoltaic Bluetooth® Low Energy Temperature Sensor Node

**JORGE ELIZALDE, CRISTINA CRUCES, MICHAEL STIVEN SANDOVAL, XABIER EGUILUZ, AND IÑAKI VAL, (Senior Member, IEEE)**

IKERLAN Technology Research Centre, Basque Research and Technology Alliance (BRTA), 20500 Arrasate-Mondragón, Spain

Corresponding author: Jorge Elizalde (jelizalde@ikerlan.es)

This work was supported by the Basque Government under Grant EDGE4IOT.

**ABSTRACT** A wireless self-powered temperature sensor node is presented. This sensor node is powered by a commercially available indoor photovoltaic energy harvester module. The sensor node uses Bluetooth® Low Energy as wireless connection. Both the hardware and firmware have been optimized to obtain a very low power consumption. An auto adaptive energy management routine has been implemented to extend the autonomy of the sensor node. The system consumption and photovoltaic generation have been characterized at different conditions, obtaining a tool to estimate the autonomy of the system. The system has also been tested in a climatic chamber to study the effect of the temperature, a key factor that affects the power consumption, and hence the autonomy of the sensor.

**INDEX TERMS** Self-powered sensor, photovoltaic generation, indoor light energy harvesting, low-power, wireless sensor, BLE.

## I. INTRODUCTION

The Bluetooth® Low Energy (BLE) radio technology has been designed for very low power consumption operations [1], [2], allowing a broad range of new Industrial IoT (IIoT) applications [3]–[5]. Taking advantage of this technology, wireless sensor nodes can operate over batteries for up to several years, depending on the final application.

At the same time, energy harvesting, and energy storage technologies have evolved improving their power and energy densities and reducing charging times [6]–[9]. With the aid of supercapacitors as energy storage components [10], energy harvesters have become a promising energy transduction technology for self-powered wireless sensor nodes.

But energy is scarce, so it is of utmost importance to collect as much energy as possible through the energy harvester and at the same time, trying to reduce as much as possible the energy consumption of the wireless sensor node [11].

The related work focuses on the technologies and architectures to, on one side maximize the harvested energy, and on the other side to minimize energy consumption. Moreover, in an industrial application there are external factors that affect the energy consumption of the device. Among them, interference sources [12], [13] and thermal variations could be very important, specifically in an industrial application.

This paper focuses on the consumption optimization of a self-powered BLE sensor node over an industrial temperature range. As far as we know, the effect of thermal variations has not been characterized in the literature. This effect has been characterized regarding on one hand the efficiency variation in the photovoltaic energy harvester module, and on the other hand the energy consumption variation of the wireless sensor node. At the same time, the power consumption has been improved through an energy management algorithm that changes the duty cycle according to the available energy.

This knowledge would enhance the life autonomy of the sensor node, as the energy storage component can be designed accordingly with the real power usage in the whole range of industrial temperatures.

The proposed system is based on a Commercial Off-The-Shelf (COTS) photovoltaic energy harvester module, optimized for indoor environments. The wireless sensor node has been designed and optimized for low energy consumption.

Both the sensor node and the reception radio module have been enclosed in a specifically designed housing to protect them against the harsh environment: dust, oil, shocks.

The associate editor coordinating the review of this manuscript and approving it for publication was Usama Mir.

The sensor node can be used in applications where there is:

- A minimum continuous light level. This scenario is typical in 24 hours places as factories, warehouses, elevators, corridors, tunnels, or car parks
- A discontinuous light level with a well-defined period of activation. This scenario is typical in places with a defined working timetable as factories, offices, public transport, or workshops

The self-powered and wireless communications features allow to use it in difficult access locations, or even not to set up a new cable installation and easily deploy a network of sensors.

This paper is organized as follows. Section II sums up related work regarding power consumption in wireless sensor nodes. Section III provides a description of the wireless sensor node and the energy harvester components. Section IV presents the system design for performance optimization in terms of energy consumption. Section V shows the performance results obtained from different setups. Finally, Section VI presents the conclusions of this work.

## II. RELATED WORK

Bouguera *et al.* [14] worked on a consumption model for sensor nodes based on Long Range LoRa® and LoRaWAN®. In the best scenario (scenario 1), sending an acceleration value every 30s, they obtained an average current consumption of 500$\mu$A.

Brunecker and Magno [15] worked on a BLE node that sends 2s of birds sound, and it is supplied by means of a radio frequency (RF) energy harvester. They obtained an average power consumption of 42.4$\mu$A.

Dementyev *et al.* [1] analyzed the current consumption of BLE, ZigBee and ANT sensor nodes in a cyclic sleep scenario. According to their results, BLE was the less power-hungry protocol. They obtained an average of 10.1$\mu$A consumption at 120s interval, and 0dBm transmission power, sending an 8-byte data packet with acknowledgement.

Dheman *et al.* [16] achieved 29$\mu$A of current consumption on a bio-impedance sensor node transmitting through Bluetooth protocol every 60s a bio-impedance measurement at 10 frequencies.

Taşkin *et al.* [17] developed a BLE sensor node for greenhouse applications, with an average current consumption of 3,23$\mu$A. In this application, the sensor node takes and sends a temperature and light measurement every 60s.

Liu *et al.* [18] designed and tested an acceleration BLE sensor node for sow behavior measurement. Sending the 3-axis acceleration every 60s, they obtained 310.57$\mu$A of current consumption. But implementing several optimizations in terms of data-grouping and sending the measurements only when there is a change in the values, they obtained a current consumption between 28.7$\mu$A and 43.5$\mu$A, depending on the sow's activity.

Yue *et al.* [19] worked on an air quality sensor node based on a photovoltaic energy harvester and a carbon dioxide ($CO_2$) sensor. The wireless communication was provided by a Moteino development platform (LoRa). They obtained a 26$\mu$A current consumption measuring every 150s.

**TABLE 1. Related work.**

| Author | Protocol | Sensor | Timing | Consumption |
|---|---|---|---|---|
| *Bouguera [14]* | LoRa® | Acceleration | 30s | 500.0µA |
| *Brunecker [15]* | BLE | Sound | 2.7h | 42.4µA |
| *Dementyev [1]* | BLE<br>ANT™<br>ZigBee | No sensor (8 bytes sent) | 120s | 10.1µA<br>28.2µA<br>15.7µA |
| *Dheman [16]* | BLE | Bio-impedance | 60s | 29.0µA |
| *Taşkin [17]* | BLE | Light & temperature | 60s | 3.2µA |
| *Liu [18]* | BLE | Acceleration | 60s | 28.7-43.5µA |
| *Yue [19]* | LoRa® | $CO_2$ | 150s | 28.3µA |
| *This work* | BLE | Temperature, Voltage & Current | 12s | 6.6µA |

There is no related work based on BLE and temperature sensing to compare. But, as it can be seen from the above table, the obtained current consumption in this work is better than most of the related work.

## III. SYSTEM ARCHITECTURE

### A. SENSOR NODE

As a starting point, a general-purpose custom prototype board has been used, removing all the expendable elements regarding this application to minimize energy wasting. The temperature sensor node is based on an BLE EFR32BG12 System on Chip (SoC) from Silicon Labs [20], and an LMT84 analog temperature sensor from Texas Instruments [21].

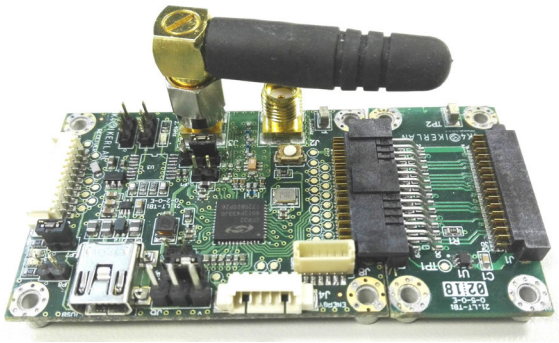

**FIGURE 1. Sensor node.**

In the following table all the components are showed, and their nominal power consumption is presented.

The firmware has been developed keeping in mind that the energy supply is limited. So, all the resources that are not used are expressly switched off. And the needed ones are activated only when used: temperature sensor and analog to digital converter.

**TABLE 2. Sensor node components.**

| Manufacturer | Component | Consumption ($V_{cc}$=3.6V) |
|---|---|---|
| *Silicon Labs* | Microcontroller - EFR32BG12-P433F1024 | Active: 468µW/MHz (130µA/MHz) Sleep: 10.5µW (2.9µA) Shut down: 3.6µW (1.0µA) |
| *Texas Instruments* | Temperature sensor - LMT84 | 19.5µW (5.4µA) |
| *Texas Instruments* | Low Drop Out regulator - TPS78236 | 1.8µW (0.5µA) |
| *EPSON* | High frequency crystal - TSX-3225-38.4 | 100µW |
| *Micro Crystal Switzerland* | Low frequency crystal – CM8V-T1A 32.768kHz | 0.5µW |

#### 1) ENERGY HARVESTER

The 4EverLast supercapacitor version of the EVL10-4V150 module has been selected [19], [22]. This module produces more power per area unit than its competitors: Panasonic Amorton, En Ocean, or PowerFilm Solar. It is composed by a 4V photovoltaic cell (high purity III-V material), a supercapacitor, and a MOSFET that switches off the output current of the module when the supercapacitor voltage drops below 3.25V.

*(a) Front*


*(b) Back*

**FIGURE 2. Photovoltaic cell.**

The energy harvester power supply module has ≈90% efficiency over a wide range of illumination levels (10-1000lux).

This module is based on Sharp technology, using the 50mm × 20mm × 1.5mm photovoltaic cell with a power density of 21.8$\mu$W/cm$^2$ (under a 200lux white light-emitting diode type illumination level) [23]. The efficiency of the solar cell is greater than 30%.

When the module is fully charged (0.5F supercapacitor), the output voltage is 4V. The module provides energy until this voltage drops below 3.25V. At this value, the module disconnects the output as an over discharge protection.

The photovoltaic module presents a quiescent charge consumed by the electronics and a leakage charge due to the supercapacitor. The quiescent current of the electronics is 2$\mu$A and the leakage current of the supercapacitor is 2$\mu$A. The consumed charge in the energy harvester module can be calculated as follows:

$$Q_q = \frac{I_q + I_{leak}}{DataRate} \tag{1}$$

In addition to the power supply connection between the sensor node and the energy harvester module, another two connections have been made to measure the voltage of the supercapacitor, and the current that is being generated in the photovoltaic cell. These two values would help the sensor node to auto adjust its performance depending on the available energy, as it is explained in the energy management section.

## IV. DESIGN

### A. ENERGY MANAGEMENT

BLE allows for a low power consumption, but there are several works intended to improve even more the energy efficiency of the system working under BLE specifications [13], [18], [24], [25]. These works dynamically change some parameters to adapt the energy consumption. In our case, the main objective of the energy management on the sensor node is to maintain it at the commanded transmission data rate as much time as possible, and secondly, to maintain it working. But this second requirement is conditioned to the main one. Similar to the Perturb & Observe (P&O) Maximum Power Point Algorithm (MPPT) used in photovoltaics to change the MOSFET duty cycle [26], here the power provided by the photovoltaic cell is monitored in each sensing cycle (voltage of the supercapacitor and current generated by the photovoltaic cell).

The energy management approach is based on 2 switching points, depending on the available energy. Therefore, 3 main operation regions are established: (i) full featured, (ii) auto adjusting and (iii) sleep. In the full featured area, there is plenty of energy and the device operates at the preprogrammed transmission data rate. In the auto adjusting area, the device reduces the transmission data rate accordingly to the available energy and the energy needed by the node. When operating in the auto adjusting region, if the energy goes up the recharge process is prioritized, and the transmission data rate is not increased until the corresponding threshold is surpassed. And finally, when the energy is not enough to maintain an appropriate working function, the device goes to sleep until the energy is restored.

### B. BLUETOOTH® LOW ENERGY

The sensor node is playing the Bluetooth® Generic Attribute Profile (GATT) server role as a slave device. It sends 3 values: temperature, super capacitor voltage, and generated photocurrent. To reduce the energy consumption, these

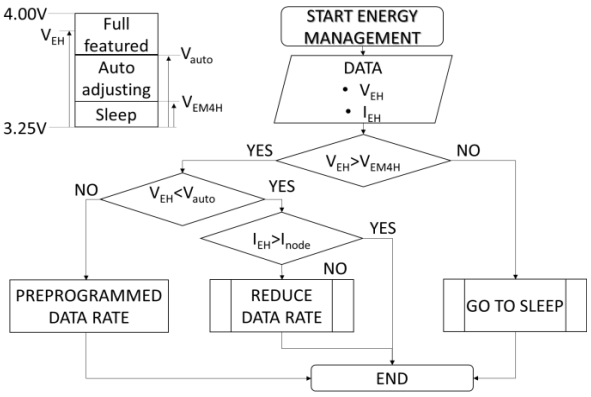


**FIGURE 3.** Energy management.

3 measured values are gathered in a single characteristic (1 transmission instead of 3).

### 1) LAZY SOFT TIMER

In BLE, a great consumption reduction is obtained going to sleep between transmissions. When a periodic action must be fulfilled, a good practice is to perform it when the microprocessor is working due to a BLE event. In this way, the overall energy usage is reduced due to sharing the energy used to awake the microprocessor between the active tasks. To synchronize the transmission event and the measurement event, the lazy soft timer has been used. This timer waits until the microprocessor is in the active state. In the following figure, the detached data transmission and measurements using the analog to digital converter (ADC) current profiles are showed in (a), and the current consumption obtained adding the detached transmission and measurement events is compared with the current consumption using the lazy soft timer to perform both events in the same awaken process (b).

In this case, the synchronization through the lazy soft timer leads to a 15% reduction in the energy consumed during the active phase.

The consumed charge by process is detailed in the following table.

**TABLE 3.** Consumed charge by process.

| Process | Charge |
|---|---|
| *Wake-up* | 0.3687µC |
| *Configuration* | 4.9405µC |
| *Transmission* | 7.2237µC |
| *Post-transmission* | 4.2033µC |
| *ADC measurements* | 5.0320µC |
| *Processing* | 2.5495µC |
| *Prepare to sleep* | 0.3539µC |
| ***TOTAL*** | **25.1715µC** |

### 2) INDICATION VS. NOTIFICATION

In the BLE protocol, indication uses a confirmation that the data transmitted has been received, meanwhile notification

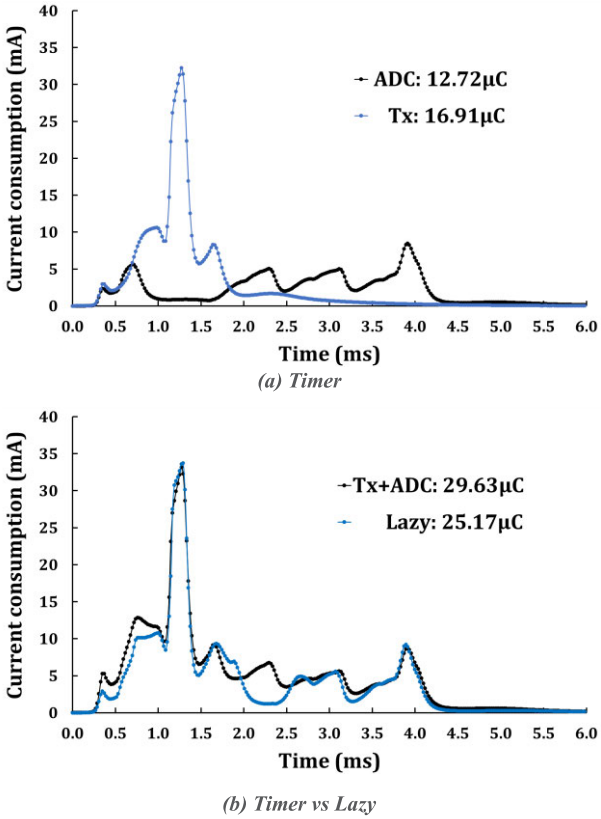


**FIGURE 4.** Current consumption profiles.

do not confirm the reception. So, indication is more robust at the expense of energy consumption. This difference has been characterized to be aware of the savings. Also, in case the application needs to be sure the data has been received by the client, we will know the impact on the autonomy of the device. We obtained the following relationships between data rate and current consumption.

$$I_{Ind}(\mu A) = 50.41 \cdot Data_{rate} + 4.75 \quad (2)$$

$$I_{Notif}(\mu A) = 35.01 \cdot Data_{rate} + 4.75 \quad (3)$$

At low transmission data rates, the difference is very low, but once this rate is over 1 data every 2 seconds (0.5data/s), indication uses around 30% to 40% more energy than notification.

In this paper we focused on very low energy consumption, so due to the energy savings, notification is going to be the selected communication method between the server and the client.

### 3) DC-DC CONVERTER

The EFR32BG12P Microcontroller Unit (MCU) has an internal optimized DC-DC converter that can be used to power the following parts: digital domain, analog domain, the analog block of the RF path, and the RF power amplifier. The DC-DC is power efficient, so it has been tested to obtain the energy savings. To measure its impact, the average

current has been measured at 3 transmission data rates: 10data/s, 5data/s, and 1data/s. Notification has been used.

As expected, the use of the internal DC-DC is mandatory to reduce the power consumption. The energy savings obtained using the internal DC-DC converter are around 30%.

The MCU can transmit at +19dBm (activating Adaptive Frequency Hopping - AFH), but this power level is not compatible with the use of the internal DC-DC converter, which greatly improves current consumption. This will impact directly in the low current consumption of the sensor node. As a reminder, the use of the DC-DC converter limits the power level to +10dBm.

#### 4) COMPILER OPTIMIZATION

The IAR compiler offers different levels of optimization: no optimization, low, medium, and high (balanced, size, and speed). In the case of high optimization, we selected the speed option, to prioritize the energy consumption reduction.

**TABLE 4. Compiler optimization effect.**

| Current consumption | 0.25data/s | 10data/s |
|---|---|---|
| *No optimization* | 27.41µA | 348.59µA |
| *Low optimization* | 24.50µA | 340.72µA |
| *Medium optimization* | 21.25µA | 334.86µA |
| *High optimization* | 18.25µA | 329.66µA |

The energy savings are highly dependent on the transmission data rate. At high transmission data rates, the energy saving is around 5%, and at low transmission data rates the energy saving is around 30%.

## V. SETUP AND RESULTS

All the measurements presented in this section have been made using a DC power analyzer Keysight N6705B, equipped with a two-quadrant source/measure unit N6781A. For temperature effect characterization, a Climats Excal 5424-HE climate chamber was used.

To evaluate the energy consumption of both the sensor node and the electronics of the energy harvester module, a charge based approach has been used [27].

### A. SENSOR NODE

#### 1) ADVERTISING

To establish the connection, the sensor node is advertising the service at +10dBm power level. In this process the consumption profile is showed, where the current peaks corresponding to the transmission over 3 channels (37, 38 and 39) are clearly visible.

During the advertising process, the current consumption has been characterized depending on the advertising rate (advertisements per second). This data would help to choose the advertising period according to the expected energy obtained by the energy harvester. The relationship is showed

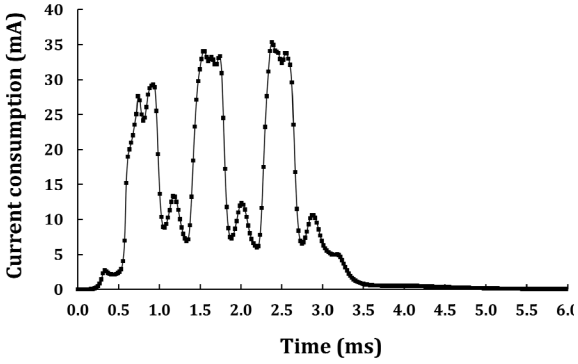


**FIGURE 5. Advertising consumption profile.**

in the next linear equation.

$$I_{adv}(\mu A) = 48.95 \cdot Adv_{rate} + 4.75 \tag{4}$$

#### 2) ACTIVE

Once the connection has been established, the sensor node sends data at the specified transmission data rate. The lazy soft timer has been used not to wake-up the MCU more than needed. When the MCU wakes-up to send the previously measured data, and then it starts the measurement of the 3 parameters using the internal ADC converter. After measuring the 3 values, the MCU gathers this information to be sent to the client in the next period and performs the energy management routine.

##### *a: POWER LEVEL*

In the following graph, the active process can be seen for 5 different RF power levels.

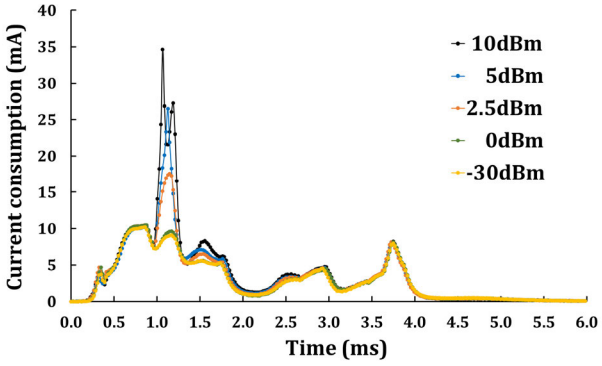


**FIGURE 6. Awake consumption profile.**

The peak current decreases rapidly between +10dBm and 0dBm, meanwhile it remains stable when the power is further reduced until −30dBm.

As it can be seen, there is a direct impact of the RF power in the consumption. In the following figure the energy consumed in the transmission process is showed.

In the processes that are RF power independent, the current consumption must be equal. The differences that can be observed are due to measurement errors. This error is ±7%.

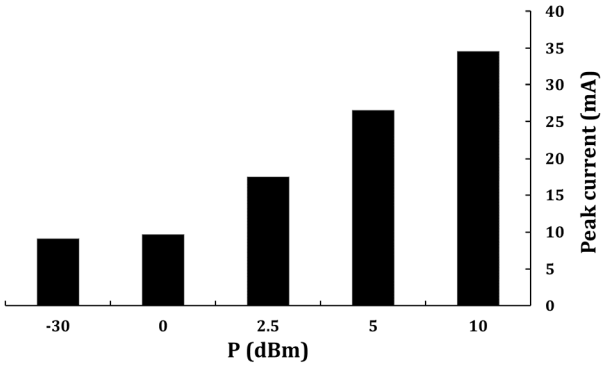


**FIGURE 7.** Peak current vs. transmission power.

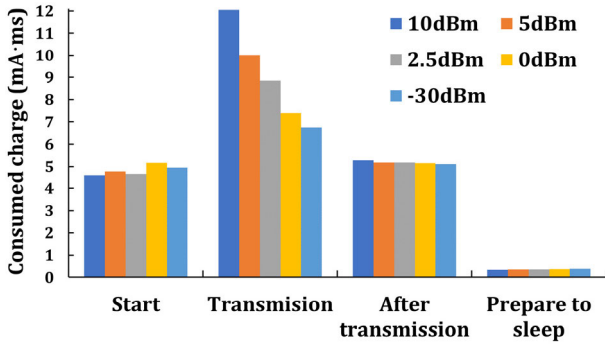


**FIGURE 8.** Consumed charge.

At a 1data/s rate, the energy consumed in the transmission process at 10dBm is the 22% of the energy consumed, whilst at 2.5dBm is a 15%, and at 0dBm is a 10%.

When the transmission data rate increases, this contribution is going to be increased.

According to these data, the system's charge consumption can be modelized according to the following equation.

$$Q_{node} = Q_{Non\ RF} + Q_{RF} + Q_{sleep} \tag{5}$$

where

- $Q_{NonRF}$ is the charge consumed in the active period, where RF is not active. So, this consumption is independent of the RF transmission power, and its value is $10.37\mu C \pm 0.21\mu C$
- $Q_{RF}$ is the charge consumed when there is transmission, and it depends on the transmission power

$$Q_{RF} = 0.458 \cdot 10^{-6} \cdot P_{RF} + 7.568 \cdot 10^{-6} \tag{6}$$

- $Q_{sleep}$ is the charge consumed when the MCU is in the sleep mode

$$Q_{sleep} = I_{sleep} \cdot \left( \frac{1}{DataRate} - t_{active} \right) \tag{7}$$

where
$I_{sleep} = 4.75\mu A$
$t_{active} = 0.010s$

### b: TRANSMISSION DATA RATE

The energy consumption of the sensor node has been characterized varying the transmission data rate at +10dBm power output. These values will be very valuable to decide the desired output data rate of the sensor node, depending on the illuminance available value.

$$I_{node}(\mu A) = 21.98 \cdot Data_{rate} + 4.75 \tag{8}$$

### c: TEMPERATURE

To characterize the current consumption with the temperature, the sensor node has been tested in a climatic chamber. The current consumption has been measured at 60°C, 40°C, 20°C, 0°C and −20°C. The sensor node was programmed at 1data/s rate and +10dBm. The average current was calculated in a 10s period, and the sleep current was measured in between 2 transmissions (990ms), at each temperature.

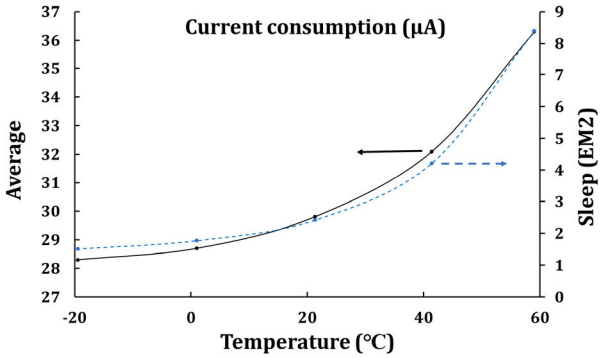


**FIGURE 9.** Sensor node current consumption in the climatic chamber.

As it can be seen, both the average current consumption and the sleep current consumption increase rapidly at temperatures higher than ambient temperature.

## B. ENERGY HARVESTER

### 1) LIGHT

The photovoltaic cell was irradiated using an 80W compact fluorescent bulb with a temperature color of 5000K. The illuminance level was measured using an RS-PRO ILM-01 light meter. The illuminance level was changed adjusting the distance between the bulb and the cell.

The following equation can be used to estimate the generated current in the cell, with a certain illumination level.

$$I_{cell}(\mu A) = 196.7 \cdot 10^{-6} \cdot E_v \tag{9}$$

The obtained relationship is in good agreement with previous related work, using the same photovoltaic module [19].

### 2) TEMPERATURE

To characterize the current generated at the photovoltaic cell at different temperatures, the cell has been tested in a climatic chamber with an 80lx illuminance level. The current generation has been measured at −20°C, 0°C, 20°C, 40°C and 60°C, and the results are showed in the next figure.

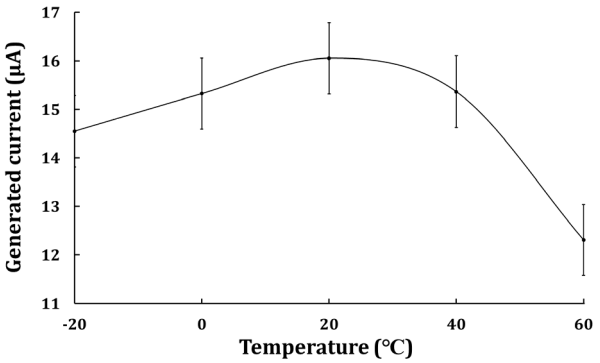


**FIGURE 10.** Climatic chamber.

The generated photocurrent has been measured through the voltage drop in the resistor located at the output of the photovoltaic cell and before the electronics. This current is reduced as temperature varies from the ambient temperature. This effect is clearer at higher temperatures.

### C. MODULE ENERGY MANAGEMENT

The advertising period has been fixed according to the energy that the photovoltaic cell can provide with a predefined minimum illuminance value (200lux). This illuminance level is usually found on corridors, and hall areas. This value could be dynamically adjusted using the energy management above mentioned, but as the advertisement is not the relevant state of the node, a fixed value is preferred.

In addition to the temperature, the voltage on the supercapacitor and the generated current are monitored to dynamically manage the consumed power. So, three measurements are made in each cycle.

To reduce the power consumption maintaining the MCU slept as much time as possible, the measurement process is synchronized with the BLE transmission, notifications are used instead of indications, and the three measurements are sent as one characteristic instead of three independent characteristics.

The sensor node is intended to be used in an industrial environment, so the module is used at an RF power output of +10dBm.

#### 1) LIGHT/TRANSMISSION DATA RATE

When the energy harvester and the sensor node are joined, we can obtain the relationship between the average illuminance level and the maximum expected transmission data rate, without using the stored energy.

The following equation can be used to estimate the maximum transmission data rate we can obtain with a certain illuminance level at ambient temperature.

$$Date\ Rate = 9.02 \cdot 10^{-3} \cdot E_v - 0.268 \tag{10}$$

#### 2) AUTONOMY

If there is no light, the autonomy of the system can be calculated using the consumption model obtained previously, and the available energy on the supercapacitor.

Until the supercapacitor goes down 3.6V, the system works at the specified transmission data rate. Then the systems adjust the transmission data rate according to the available energy. The system is going to hibernate mode when the voltage is lower than 3.3V. So, we have 3 regions: full speed, reduced speed and hibernate.

The consumed charge in the module is the sum of the sensor node consumption (Eq. 5) and the leakage on the energy harvester module (Eq. 1).

$$Q = Q_{sensor} + Q_q \tag{11}$$

Using Eq. 11, the autonomy can be easily calculated at different transmission data rates and transmission power levels considering:

- Full featured region: the voltage of the supercapacitor decreases from 4.0V until 3.6V. The theoretically charge supplied by the supercapacitor in this range of voltages is 0.20C
- Auto adjusting region: the voltage of the supercapacitor decreases from 3.6V until 3.3V. The theoretically charge supplied by the supercapacitor in this range of voltages is 0.15C.
- Hibernate region: when the voltage is less than 3.3V, the system enters the hibernate state, and the current consumption is reduced to 0.9$\mu$A.

In the following figure, the voltage of the supercapacitor is showed at night, when the lights are switched off. In this test, the sensor node is programmed at 2data/s, and where it is placed the illuminance level is 900lx. There are 7 regions:

a) Lights are on: the supercapacitor is fully charged, and the sensor node is working at programmed transmission data rate (2data/s)
b) Lights are off and $V_{Supercap} > 3.6V$: the sensor node is working at programmed transmission data rate (2data/s)
c) Lights are off and $V_{Supercap} < 3.6V$: the sensor node is adapting the transmission data rate accordingly to the generated current. In this region there is no generated current, so the sensor node decreases the data rate until it reaches the programmed minimum data rate (1 data every 12s)
d) Lights are off and $V_{Supercap} < 3.3V$: the sensor node goes to hibernate mode. Due to the long time without light, the voltage reaches the minimum 3.25V. At this voltage, the energy harvester module switches off the MOSFET, and the sensor node becomes unpowered
e) Lights are on: the energy harvester module is charging the supercapacitor, but the sensor node is not powered
f) Lights are on: the energy harvester module switches on its MOSFET when the voltage of the supercapacitor is greater than 3.48V. Once this threshold has been overtaken, the sensor node awakes. There's plenty of light, so the sensor node starts working at the programmed transmission data rate (2data/s)

g) Lights are on: the supercapacitor is fully charged, and the sensor node is working at programmed transmission data rate (2data/s)

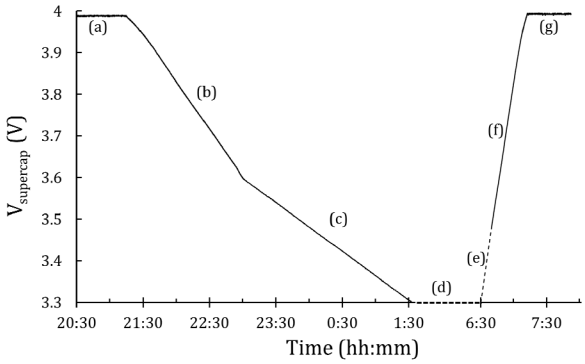


**FIGURE 11.** Test of the wireless sensor node.

### 3) CHARGING TIME

The charging time can be easily estimated using equations 8 and 9, and it depends on the initial status of the module, and the illumination and data rate levels.

In this application, the easiest way to calculate the charging time is by using the charge of the supercapacitor at each voltage level.

$$q = C \cdot V \tag{12}$$

The charging time is calculated by dividing the charge increase by the allowable current to charge the supercapacitor. This charge current is the difference between the generated current in the photovoltaic cell and the current consumption on the sensor node.

$$t = \frac{C \cdot (V_1 - V_0)}{I_{cell} - I_{node}} \tag{13}$$

In the following table the charging process times are compared between the above-mentioned test case (figure 11), and the previous formula.

**TABLE 5.** Charging time comparison.

| Charging time (minutes) | Test | Estimation |
|---|---|---|
| *Unpowered sensor node (e)* | 10 | 11 |
| *Programmed data rate (f)* | 32 | 33 |

### 4) ENCLOSURE

An enclosure has been designed and built for the node sensor and the receptor unit to protect the devices against dust, oil, and small shocks. Both enclosures have been manufactured using a stereolithography system.

Both enclosures have been designed with fastening straps to help in the fixation process.

#### *a: WIRELESS SENSOR NODE*

The enclosure for the Self-Powered Sensor has a big window for the photovoltaic cell, and a small one for the antenna. There is also a light guide to have a visual feedback. A blue light switches on every time there is a data transmission process.


**FIGURE 12.** Enclosure of the wireless sensor node.

#### *b: RECEIVER*

This enclosure has two small holes, one for the antenna and the other one for the USB cable. The USB cable is used to transfer the received data to the computer. There are also two light guides to have a visual feedback of the receiver: a blinking red light where the receiver is searching for sensor nodes, and a blue light when the receiver is receiving new data coming from the sensor node.


**FIGURE 13.** Enclosure of the receiver.

### 5) GRAPHICAL USER INTERFACE

A graphical user interface has been developed using LabVIEW from National Instruments. The purpose of this interface is to show the relevant parameters of the sensor node: temperature, voltage of the supercapacitor, current generation on the photovoltaic module, and the Received Signal Strength Indicator (RSSI) of the connection.

In the following figure, it can be seen how a greater illumination level (generated current-red line in the upper left graph), leads to a higher voltage increase rate (bottom left graph).

An infrared lamp has been used to heat the sensor up, as it can be seen in the right graph (temperature increase).

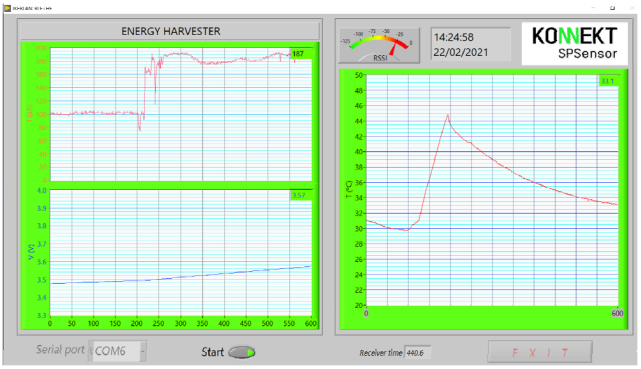


**FIGURE 14.** Graphical user interface.

## VI. CONCLUSION

A Bluetooth® Low Energy temperature sensor node has been developed to be able to work with an indoor photovoltaic energy harvester as a sole energy source.

This sensor node is going to be used in an industrial environment, so the behavior of the whole system has been characterized in a climatic chamber between −20°C and +60°C.

Several parameters have been analyzed to better understand the effect of them in the power usage of the node.

As a result, a relationship between transmission power, data-transmission rate, and the expected autonomy has been obtained, allowing the main objective: maximize the autonomy of the sensor node.

The strategy was to develop an energy management tool based on 3 working zones: full featured transmission data rate, auto adjusting data rate and sleep. In the full featured data rate zone, the sensor node is working at the maximum expected data rate. In the auto adjusting data rate zone, the sensor node auto adjusts the data rate based on the available energy and the power consumption at that data rate. And finally, when the available energy is not enough to guarantee an acceptable autonomy, the sensor node goes to a sleep state to consume the less possible amount of energy waiting for more energy to come. In this sleep state, the only part that is awake is the voltage monitor to check when to awake the MCU.

In the future, this module can be updated to sense other parameters by changing the sensor module of the sensor node: acceleration, pressure, air quality, presence detection, strain, or magnetic field.

## ACKNOWLEDGMENT

The authors would like to thank David García Barrio for his assistance in climate chamber tests and the design of the enclosures.

## REFERENCES

[1] A. Dementyev, S. Hodges, S. Taylor, and J. Smith, "Power consumption analysis of Bluetooth low energy, ZigBee and ANT sensor nodes in a cyclic sleep scenario," in *Proc. IEEE Int. Wireless Symp. (IWS)*, Apr. 2013, pp. 1–4, doi: 10.1109/IEEE-IWS.2013.6616827.

[2] M. Siekkinen, M. Hiienkari, J. K. Nurminen, and J. Nieminen, "How low energy is Bluetooth low energy? Comparative measurements with ZigBee/802.15.4," in *Proc. IEEE Wireless Commun. Netw. Conf. Workshops (WCNCW)*, Apr. 2012, pp. 232–237, doi: 10.1109/WCNCW.2012.6215496.

[3] J. Yang, C. Poellabauer, P. Mitra, and C. Neubecker, "Beyond beaconing: Emerging applications and challenges of BLE," *Ad Hoc Netw.*, vol. 97, Feb. 2020, Art. no. 102015, doi: 10.1016/j.adhoc.2019.102015.

[4] A. H. Omre and S. Keeping, "Bluetooth low energy: Wireless connectivity for medical monitoring," *J. Diabetes Sci. Technol.*, vol. 4, no. 2, pp. 457–463, Jan. 2010, doi: 10.1177/193229681000400227.

[5] K. Maneerat and K. Kaemarungsi, "Performance improvement design of Bluetooth low energy-based wireless indoor positioning systems," *Mobile Inf. Syst.*, vol. 2020, Dec. 2020, Art. no. 8891856, doi: 10.1155/2020/8891856.

[6] K. S. Adu-Manu, N. Adam, C. Tapparello, H. Ayatollahi, and W. Heinzelman, "Energy-harvesting wireless sensor networks (EH-WSNs): A review," *ACM Trans. Sensor Netw.*, vol. 14, no. 2, Jul. 2018, Art. no. 10, doi: 10.1145/3183338.

[7] H. Elahi, K. Munir, M. Eugeni, S. Atek, and P. Gaudenzi, "Energy harvesting towards self-powered IoT devices," *Energies*, vol. 13, no. 21, p. 5528, Oct. 2020, doi: 10.3390/en13215528.

[8] I. Mathews, S. N. Kantareddy, T. Buonassisi, and I. M. Peters, "Technology and market perspective for indoor photovoltaic cells," *Joule*, vol. 3, no. 6, pp. 1415–1426, 2019, doi: 10.1016/j.joule.2019.03.026.

[9] P. Choudhary, L. Bhargava, V. Singh, M. Choudhary, and A. K. Suhag, "A survey—Energy harvesting sources and techniques for Internet of Things devices," *Mater. Today*, vol. 30, no. 1, pp. 52–56, 2020, doi: 10.1016/j.matpr.2020.04.115.

[10] J. Libich, J. Máca, J. Vondrák, O. Čech, and M. edlaříková, "Supercapacitors: Properties and applications," *J. Energy Storage*, vol. 17, pp. 224–227, Jun. 2018, doi: 10.1016/j.est.2018.03.012.

[11] T. Rault, A. Bouabdallah, and Y. Challal, "Energy efficiency in wireless sensor networks: A top-down survey," *Comput. Netw.*, vol. 67, pp. 104–122, Jul. 2014, doi: 10.1016/j.comnet.2014.03.027.

[12] M. O. Al Kalaa, W. Balid, N. Bitar, and H. H. Refai, "Evaluating Bluetooth low energy in realistic wireless environments," in *Proc. IEEE Wireless Commun. Netw. Conf.*, Apr. 2016, pp. 1–6, doi: 10.1109/WCNC.2016.7564809.

[13] M. Spörk, C. A. Boano, and K. Römer, "Improving the timeliness of Bluetooth low energy in noisy RF environments," presented at the Int. Conf. Embedded Wireless Syst. Netw., Beijing, China, 2019. [Online]. Available: https://dl.acm.org/doi/10.5555/3324320.3324324

[14] T. Bouguera, J.-F. Diouris, J.-J. Chaillout, R. Jaouadi, and G. Andrieux, "Energy consumption model for sensor nodes based on LoRa and LoRaWAN," *Sensors*, vol. 18, no. 7, p. 2104, Jun. 2018, doi: 10.3390/s18072104.

[15] O. Brunecker and M. Magno, "TinyBird: An energy neutral acoustic Bluetooth-low-energy sensor node with RF energy harvesting," in *Proc. 7th Int. Workshop Energy Harvesting Energy-Neutral Sens. Syst.* New York, NY, USA: Association for Computing Machinery, 2019, pp. 1–7, doi: 10.1145/3362053.3363498.

[16] K. Dheman, P. Mayer, M. Eggimann, S. Schuerle, and M. Magno, "ImpediSense: A long lasting wireless wearable bio-impedance sensor node," *Sustain. Comput., Informat. Syst.*, vol. 30, Jun. 2021, Art. no. 100556, doi: 10.1016/j.suscom.2021.100556.

[17] D. Taşkin, C. Taskin, and S. Yazar, "Developing a Bluetooth low energy sensor node for greenhouse in precision agriculture as Internet of Things application," *Adv. Sci. Technol. Res. J.*, vol. 12, no. 4, pp. 88–96, 2018, doi: 10.12913/22998624/100342.

[18] L.-S. Liu, J.-Q. Ni, R.-Q. Zhao, M.-X. Shen, C.-L. He, and M.-Z. Lu, "Design and test of a low-power acceleration sensor with Bluetooth low energy on ear tags for sow behaviour monitoring," *Biosyst. Eng.*, vol. 176, pp. 162–171, Dec. 2018, doi: 10.1016/j.biosystemseng.2018.10.011.

[19] X. Yue, M. Kauer, M. Bellanger, O. Beard, M. Brownlow, D. Gibson, C. Clark, C. MacGregor, and S. Song, "Development of an indoor photovoltaic energy harvesting module for autonomous sensors in building air quality applications," *IEEE Internet Things J.*, vol. 4, no. 6, pp. 2092–2103, Dec. 2017, doi: 10.1109/JIOT.2017.2754981.

[20] Silicon Labs. *EFR32BG12*. Accessed: 2021. [Online]. Available: https://www.silabs.com/wireless/bluetooth/efr32bg12-series-1-socs

[21] Texas Instruments. *LMT84*. Accessed: 2021. [Online]. Available: https://www.ti.com/product/LMT84

[22] Lightricity Ltd. *4EverLast EVL10-4V150*. Accessed: 2021. [Online]. Available: https://lightricity.co.uk/4everlast-exl10-4v150
[23] Lightricity Ltd. *ExCellLight EXL10-4V170*. Accessed: 2021. [Online]. Available: https://lightricity.co.uk/excelllight-exl10-4v170/
[24] E. Park, M.-S. Lee, H.-S. Kim, and S. Bahk, "AdaptaBLE: Adaptive control of data rate, transmission power, and connection interval in Bluetooth low energy," *Comput. Netw.*, vol. 181, Nov. 2020, Art. no. 107520, doi: 10.1016/j.comnet.2020.107520.
[25] M. Collotta and G. Pau, "Bluetooth for Internet of Things: A fuzzy approach to improve power management in smart homes," *Comput. Elect. Eng.*, vol. 44, pp. 137–152, May 2015, doi: 10.1016/j.compeleceng.2015.01.005.
[26] A. Haque, "Maximum power point tracking (MPPT) scheme for solar photovoltaic system," *Energy Technol. Policy*, vol. 1, no. 1, pp. 115–122, Jan. 2014, doi: 10.1080/23317000.2014.979379.
[27] X. Yue, J. Kiely, D. Gibson, and E. M. Drakakis, "Charge-based supercapacitor storage estimation for indoor sub-mW photovoltaic energy harvesting powered wireless sensor nodes," *IEEE Trans. Ind. Electron.*, vol. 67, no. 3, pp. 2411–2421, Mar. 2020, doi: 10.1109/TIE.2019.2896321.

**JORGE ELIZALDE** was born in Donostia/San Sebastián, Gipuzkoa, Spain, in 1968. He received the B.S., M.S., and Ph.D. degrees in industrial engineering from the University of Navarra, Donostia/San Sebastián, Gipuzkoa, in 1992, 1994, and 1997, respectively.

From 1997 to 1999, he worked with the Clínica Universidad de Navarra. Since 1999, he has been a Researcher with IKERLAN, Arrasate/Mondragón, Gipuzkoa. From 1999 to 2017, he worked at Microsystems Area. His research interests included lithography, electrochemical microsensors, microfluidics, soft lithography, and smart systems. Since 2019, he has been working with the Communications Systems Group. His research interests include low-power wireless sensors and bluetooth® low energy. He is the author of 55 articles and five inventions.

**CRISTINA CRUCES** received the B.S. degree in telecommunications engineering from the Faculty of Engineering of Bilbao, University of the Basque Country UPV/EHU, in 2006.

Since 2006, she has been a Researcher with Communications Systems Group, IKERLAN, Arrasate/Mondragón, Gipuzkoa, Spain. She has collaborated with the Applied Electronic Group (APERT), Department of Telecommunications, University of the Basque Country UPV/EHU, from 2003 to 2006, on the development of a wireless sensor mac and network protocol. In the last years, she has focused the research activities on low-power wireless sensor networks, ethernet real time, and industrial wireless communications. She is the author of eight articles.

**MICHAEL STIVEN SANDOVAL** received the M.Sc. degree in embedded systems engineering from the Faculty of Informatics of Donostia/San Sebastián, University of the Basque Country UPV/EHU, in 2019.

He has been a member of IKERLAN, Arrasate/Mondragón, Gipuzkoa, Spain, since 2018, where he began as intern and carried out his master's thesis in energy optimization on low-power systems. Since 2019, he has been working as a Researcher with Hardware Systems Group towards the development of systems focused on energy efficiency, definition of low energy software and firmware architectures, implementation of embedded HW-SW units based on analysis of specifications and technical documentation, and functional validation of custom HW designs.

**XABIER EGUILUZ** received the B.S. degree in telecommunications engineering and the Ph.D. degree from the University of Deusto, Spain, in 2008 and 2016, respectively.

Since 2008, he has been working as a Researcher with DeustoTech-University, Deusto, participating in projects related to wireless sensor networks and energy harvesting systems applied to low power electronics. He has carried out several internships with Fraunhofer Institute IIS, Nuremberg, Germany. Since 2016, he has been with the Hardware and Communication Systems Area, IKERLAN. There, he has participated in several national and international research projects involving low-powered sensor systems and wireless communications systems for harsh environments.

**IÑAKI VAL** (Senior Member, IEEE) received the B.Sc. and M.Sc. degrees from the Department of Electronics Engineering, University of Mondragon, Spain, in 1998 and 2001, respectively, and the Ph.D. degree from the Department of Signals, Systems, and Radiocommunication, Polytechnic University of Madrid, Spain, in 2011.

Since 2001, he has been with Communications Systems Group, IKERLAN, Arrasate/Mondragón, Gipuzkoa, Spain. He was with Fraunhofer Institute for Integrated Circuits IIS, Erlangen, Germany, as an Invited Researcher, from 2005 to 2006. He is currently the Team Leader of the Communication Systems Group. He is currently focused on industrial communication applications. His research interests include design and implementation of digital wireless communications systems, industrial real-time requirements, communications for distributed control systems, vehicular communications, time synchronization, wireless channel characterization, and digital signal processing.